Applied Catalysis B: Environmental 148–149 (2014) 543–549

Contents lists available at ScienceDirect

Applied Catalysis B: Environmental

journal homepage: www.elsevier.com/locate/apcatb

Influence of colloidal graphene oxide on photocatalytic activity of nanocrystalline TiO_2 in gas-phase ethanol and benzene oxidation

Natalya S. Andryushina, Oleksandr L. Stroyuk*

L.V. Pysarzhevsky Institute of Physical Chemistry of National Academy of Sciences of Ukraine, 31 Nauky av., 03028, Kyiv, Ukraine

ARTICLE INFO

Article history:
Received 12 September 2013
Received in revised form
22 November 2013
Accepted 25 November 2013
Available online 1 December 2013

Keywords:
Semiconductor photocatalysis
Partially reduced graphene oxide
Titania-graphene nanocomposites
Volatile pollutants

ABSTRACT

Impregnation of the nanocrystalline TiO_2 Degussa/Evonik P25 by colloidal graphene oxide produced by the Hummers method (H-GO) results in a 4-fold acceleration of photocatalytic gas-phase oxidation of ethanol and benzene vapors by air oxygen as a result of enhanced separation of the photogenerated charge carriers between TiO_2 and H-GO. Preliminary photochemical reduction of H-GO decreases drastically its activity in ethanol photooxidation but does not affect appreciably photocatalytic oxidation of benzene. More deeply oxidized colloidal GO produced by the Brodie method (B-GO) almost does not affect the photocatalytic properties of titania in benzene photooxidation. It is concluded that the catalytic properties of GO in the photooxidation of ethanol and benzene depend on a balance between the capabilities of the GO sheets (i) to accept photoelectrons from titania nanocrystals and (ii) to bound to the TiO_2 surface. The former factor depends on the aromaticity of GO particles and increases from B-GO to H-GO to photoreduced H-GO, while the latter factor depends on the density of the functional groups on GO sheets and increases in the opposite direction.

1. Introduction

Enhancement of the photocatalytic activity of nanocrystalline semiconductors and/or expansion of the spectral sensitivity range of such materials can be achieved by combining a photocatalyst with dyes, metal complexes, nanocrystals (NCs) of metals or other semiconductors, conjugated polymers, and various forms of carbon–carbon nanotubes, fullerenes, graphene oxide (GO) and partially reduced GO (pr-GO) [1–3]. The two latter objects, which have attracted a considerable interest in recent years [4–7], play a multiple role in the semiconductor-based photocatalytic systems. In particular, the GO and pr-GO sheets can accept photogenerated conduction band electrons from the semiconductor suppressing the electron-hole recombination, and impart the semiconductor with capability of selective adsorption of aromatic molecules via ππ-stacking interactions with the aromatic sp^2-hybridized carbon areas of the GO (pr-GO) sheets [1–3,8,9]. As a result, for example, the TiO_2/pr-GO heterostructures serve as efficient photocatalysts of decomposition of dyes [10–16], oxidation of benzene [13], benzyl alcohols [17,18], acetone [9] and trichloroacetic acid [19], as well as reduction of Cr(VI) [15], CO_2 [20], CO [21], and water [8,22–24]. In some cases, conjugation of the pr-GO sheets with wide-band-gap semiconductor NCs, such as TiO_2, ZnO or ZnS, impart the semiconductor with sensitivity to the visible light as a result of metal-carbon bonds formation on the NC surface [10,11] or a spectral sensitization effect [25]. Finally, when the pr-GO based heterostructures are synthesized by the solvothermal treatment, the GO sheets often act as a structure-directing agent affecting the NC size, shape and phase composition of the produced nanocrystalline materials [2,13,22,26–28].

It is well established that reduction of GO affects strongly its properties, in particular, the conductivity, electron transition energy, the charge carriers dynamics, electron affinity, *etc.* [4,5]. A number of reduction methods was introduced allowing to vary the properties of pr-GO, for example, controlled contact of GO with strong reducing agents [19], photochemical reduction [16,19,29–33], microwave or ultrasound treatment [4,20,34], *etc.* Obviously, modification of the GO properties in the course of reduction should affect considerably the activity of pr-GO as a co-catalyst in the semiconductor photocatalytic systems. However, analysis of recent literature shows that relationships between the "depth" of pr-GO reduction and its ability to accelerate photocatalytic reactions on the surface of semiconductor NCs remain still to be explored. Apparently, the lack of data originates from the fact that in most cases the composite photocatalysts are prepared by the solvothermal treatment [8–10,12–15,22,24,26,28,35–37] when formation of semiconductor NCs, GO reduction and conjugation of the NCs and pr-GO into a heterostructure occur simultaneously and can not be discriminated [2,10,13]. By this reason, in these papers

* Corresponding author. Tel.: +380 44 5250270; fax: +380 44 5250270.
E-mail addresses: stroyuk@inphyschem-nas.kiev.ua, alstroyuk@ukr.net (O.L. Stroyuk).

0926-3373/$ – see front matter © 2013 Elsevier B.V. All rights reserved.
http://dx.doi.org/10.1016/j.apcatb.2013.11.044

the photocatalytic properties of NCs/pr-GO heterostructures are compared not with those of similar NC/GO heterostructures, but rather with the properties of semiconductor NCs synthesized without additions of GO.

In this view, a comparison of the photocatalytic properties of heterostructures produced by mechanical mixing of nanocrystalline semiconductors with the GO or pre-synthesized pr-GO seems to be a more correct way of establishing the relationships between the reduction state and catalytic activity of GO and pr-GO sheets [17,21,38]. However, in rare papers, where this methodology is applied, the authors compare the photocatalytic properties of the heterostructures based on pr-GO and another carbon material – the multi-wall carbon nanotubes (MWCNTs) [12,13,17,18,39] and typically do not present the data for the GO-based heterostructures.

In most cases the organic dyes are used as model substrates in such systems [1,2,10–16,26,29,35,38]. Typically, the dyes exhibit excellent adsorption on the pr-GO sheets which can mask any possible changes in the properties and, therefore, catalytic activity of pr-GO resulting from variations in the pr-GO reduction depth. So, the pr-GO-based heterostructures should be tested not only in the photocatalytic transformations of aromatic substrates, such as dyes, but also as photocatalysts of oxidation/reduction of non-aromatic species that do not adsorb selectively on the aromatic areas of the pr-GO sheets.

Among the semiconductor-mediated photoprocesses the gas-phase photocatalytic decomposition of volatile organic compounds is of obvious applied interest as a promising tool of dealing with air pollution. In a survey performed in 1998 by the US Environmental Protection Agency [40] benzene, ethanol and acetaldehyde were indicated as three of five of the most common volatile air pollutants. Ethanol is constantly used as part of disinfectants and aseptic solutions and emitted in considerable amounts in bakery and brewery industries. Benzene is widespread as a component of motor fuels and has high carcinogenic activity and a low permissible exposure limit of 1 ppm [41]. The processes of photocatalytic oxidation of ethanol [42–48] and benzene [13,49–55] are often used as model gas-phase reactions to test and compare the photoactivity of various semiconductors and composite materials.

The present paper reports a comparative study of the photocatalytic properties of the heterostructures produced by impregnation of nanocrystalline TiO_2 Degussa/Evonik P25 by aqueous colloids of GO and photochemically reduced pr-GO in reactions of the gas-phase oxidation of ethanol and benzene vapors by air oxygen.

2. Experimental

Graphite powder (Merck), concentrated H_2SO_4, $KMnO_4$, aqueous 30 wt.% H_2O_2 solution, HCl, reagent-grade benzene (Sigma–Aldrich), nanocrystalline TiO_2 P25 (Evonik/Degussa Corp.) were used as supplied. Graphite oxide was synthesized by the well-known modified Hummers method via graphite oxidation by sodium permanganate in concentrated sulfuric acid [4]. The graphite oxide synthesized by the Brodie method via graphite oxidation by $KClO_3$ [4] was kindly supplied by Dr. M.V. Savoskin and E.S. Papayanina (L.M. Lytvynenko Institute of Physical Organic Chemistry and Coal Chemistry, National Academy of Sciences of Ukraine). By the ultrasound-assisted exfoliation of the graphite oxide powders of both types in distilled water (ultrasound disperser UZDN-A, 130 W, 22 kHz, Ukraine) colloidal graphene oxide was prepared with the concentration of up to 500 mg/L as described in [30]. The GO colloids produced from the Hummers- and Brodie-graphite oxide are further denoted as H-GO and B-GO, respectively.

Photochemical experiments were carried out using the focused light from a 1000 W high-pressure mercury lamp cut-filtered to the range of $\lambda = 310–390$ nm using a combination of standard optical filters. The integral light intensity was 25 mW/cm^2. A 50.0-mm glass cuvette with water was placed between the light source and a work reactor to avoid heating of the latter.

The photochemically reduced GO (pr-GO) was prepared similarly to [30] by illuminating the degassed colloidal GO in a 10.0-mm quartz cuvette for 3 h. The composite titania-based photocatalysts were prepared by suspending 0.1 g TiO_2 in colloidal GO solution (typically 10 mL of 500 mg/L GO solutions were used to obtain samples with 5 wt.% GO). The suspension was refluxed for 1 h at room temperature and left for the water evaporation in a Petri dish to obtain a powdered photocatalyst. The mixtures of TiO_2 with graphite, graphite oxide, and MWCNTs (5 wt.%) were prepared by mechanical grinding of dry components in an agate mortar. The MWCNTs were kindly supplied by Prof. P.E. Strizhak and Dr. N.V. Lemesh (L.V. Pysarzhevsky Institute of Physical Chemistry, National Academy of Sciences of Ukraine). The MWCNTs were synthesized and purified by treatment with concentrated HNO_3 similarly to [56].

Photocatalytic processes were studied in a glass 130-mL reactor (oxidation of ethanol and acetaldehyde) or a quartz 35-mL reactor (benzene oxidation). The photocatalyst (0.05 g) pressed as a tablet was placed in the reactor center, then an aliquot of the liquid substrate (96 vol.% ethanol or benzene) was injected through a septum into the reactor by a micro-syringe. The reactor content was kept in dark for 200 min with continuous magnetic stirring to reach the adsorption/desorption equilibrium. The ethanol and acetaldehyde concentrations were determined by gas chromatography, the samples taken through a septum by a micro-syringe. The benzene concentration was determined by spectrophotometry from the intensity of the 0-0 vibrational peak of the benzene absorption band (at $\lambda = 267$ nm). Absorption spectra were recorded on a Specord 200 spectrophotometer directly in the quartz reactor. Scanning electron microscopic (SEM) images of the samples were obtained on a Tescan Mira 3 microscope at an accelerating voltage of 20 kV.

3. Results and discussion

3.1. Characterization of H-GO and TiO_2/H-GO

Oxidation of graphite by the Hummers method results in extinction of the characteristic XRD peak of graphite at 26.5° (3.5 Å) [4,5,57,58] (Fig. 1a, curve 1) and rise of a new peak at 10.6° (8.3 Å) belonging to graphite oxide (Fig. 1a, curve 2) [4,59]. Expansion of the interlayer space in graphite oxide, as compared to graphite, is caused by introduction of various oxygen-containing functional groups (epoxides, hydroxyls, carboxyls) to graphene sheets as a result of oxidative etching [4,5]. The ultrasound treatment of the powdered graphite oxide in distilled water results in exfoliation of the powder and formation of stable and transparent colloidal solutions.

The XRD spectra of the powders obtained by water evaporation from the colloidal solutions exhibit a residual reflex at 8–10°, its intensity being by an order of magnitude lower than the corresponding peak of the starting graphite oxide (Fig. 1a, curve 3). The fact shows that the ultrasound treatment results in almost complete exfoliation of graphite oxide and formation of monolayer graphene oxide (GO) with some residual fraction (around 10%) of multilayer particles still present in the solution. AFM shows that the colloidal solutions contain planar sheet-like particles with the lateral size from tens of nanometers to several microns (Fig. 1b) and a thickness of 1.2–1.5 nm (inset in Fig. 1b). The sheet thickness falls into the range typical for monolayer GO, from 0.6 nm to 1.6 nm, depending on the humidity and the sample history [6,60,61].

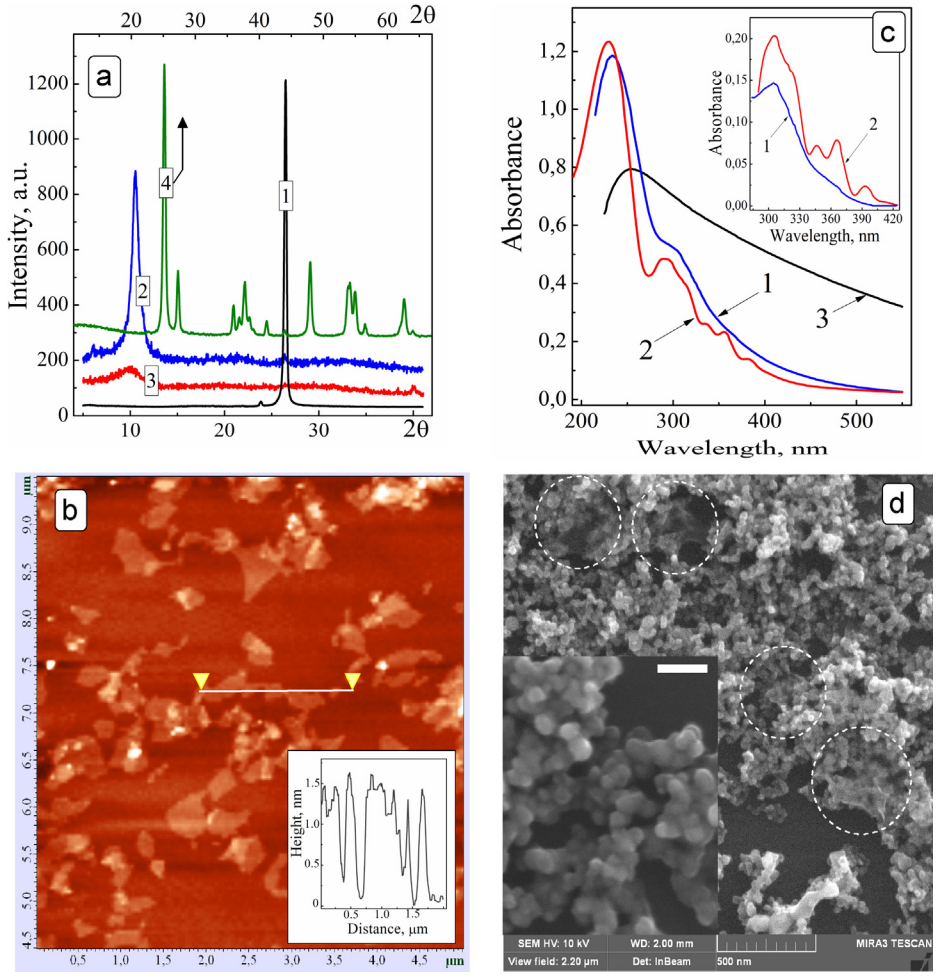

Fig. 1. (a) XRD spectra of graphite powder (curve 1), graphite oxide powder (curve 2), H-GO particles (curve 3), and TiO_2 Evonik/Degussa P25 (curve 4). The *X*-axis for curves 1–3 is given in the lower part of the figure, while that for the curve 4 – in the upper part of the figure. (b) AFM image of H-GO sheets. Inset: a cross-section of the AFM image (the cross-section direction is shown by line and triangles on the main figure). (c) Absorption spectra of colloidal H-GO (curve 1), B-GO (curve 2), and photoreduced H-GO (curve 3). [GO] = 5×10^{-4} M, cuvette −10.0 mm. Inset: $n\pi$-absorption bands of colloidal H-GO (curve 1) and B-GO (curve 2). (d) SEM of TiO_2/H-GO composite. Circles show H-GO sheets surrounded by titania NCs. Inset: SEM of pure TiO_2 P25, the scale bar is 100 nm.

Absorption spectra of colloidal GO exhibit a peak at 230–240 nm (Fig. 1c, curves 1 and 2), typical for graphite, graphene and products of graphene oxidation. In case of graphene the peak is observed at 270 nm and typically assigned to the van Hove singularity of states in slightly crumpled graphene sheets [5,62]. Oxidation of the graphene sheets results in a "blue" shift of the characteristic peak the more pronounced the deeper is the oxidation state of the graphene and the smaller is a fraction of residual aromatic sp^2-hybridized carbon atoms in the GO sheets [5,62]. In a longer wavelength region, at $\lambda > 290$ nm, a shoulder is observed originating from the $n\pi$-type electron transitions in carboxyl and phenol groups of GO [4,5], its intensity and shape depending on the amount and nature (the nearest environment) of the groups. Absorbance in the range of $\lambda > 400$ nm originates from the electron excitation of aromatic sp^2-hybridized areas of GO sheets that avoided oxidation. As shown by the present authors in [30], photoexcitation of the aromatic subsystem of the H-GO sheets results in the indirect electron transitions with a minimal energy of 1.9–2.0 eV.

A comparison of the absorption spectra of H-GO and B-GO colloids reveals a series of spectral features indicating that B-GO sheets are oxidized more deeply as compared to the H-GO sheets. In particular, a characteristic absorption maximum of the B-GO colloids is shifted to shorter wavelengths relative to H-GO. The fact, along with a higher absorbance of the H-GO in the range of $\lambda > 400$ nm, indicates that the H-GO sheets have a more developed and extensive aromatic system as compared to B-GO.

In the range of $n\pi$-absorbance the B-GO reveals a complex superposition of several $n\pi$-bands (Fig. 1c, curve 2), while the less-oxidized H-GO exhibits here only a low-intensity shoulder on the onset of the main spectral maximum (curve 1). A contribution of the $n\pi$-absorbance can be extracted by subtracting both the van Hove maximum at 230–240 nm and the longer-wavelength band of the indirect transitions in the aromatic sp^2-clusters of the GO sheets from the original absorption spectra of colloidal GO solutions. The subtraction was performed as follows. A section of the spectrum at $\lambda > 400$ nm ($h\nu < 3.1$ eV) was linearized in the coordinates of the Tauc plot for indirect transitions, $(D \times h\nu)^{1/2} - h\nu$, then the obtained linear dependence was extrapolated to $h\nu = 6.5$ eV and original $D(h\nu)$ spectrum was reconstructed in the range of $h\nu < 6.5$ eV. The as-extrapolated $D(h\nu)$ curve corresponds solely to the absorbance due to electronic excitation of the aromatic subsystem. The maximum at 230–240 nm originating from the van Hove resonance [63] can be fitted by a Lorenz curve. Fig. 1c (inset) shows results of the subtraction of both the Lorenz peak and the extrapolated $D(h\nu)$ curve from the original absorption spectra of colloidal GO solutions. The inset in Fig. 1c presents solely $n\pi$-absorbance of GO sheets. The integral $n\pi$-absorbance in the range of 300–420 nm in case of B-GO was found to be almost 2 times higher than for H-GO

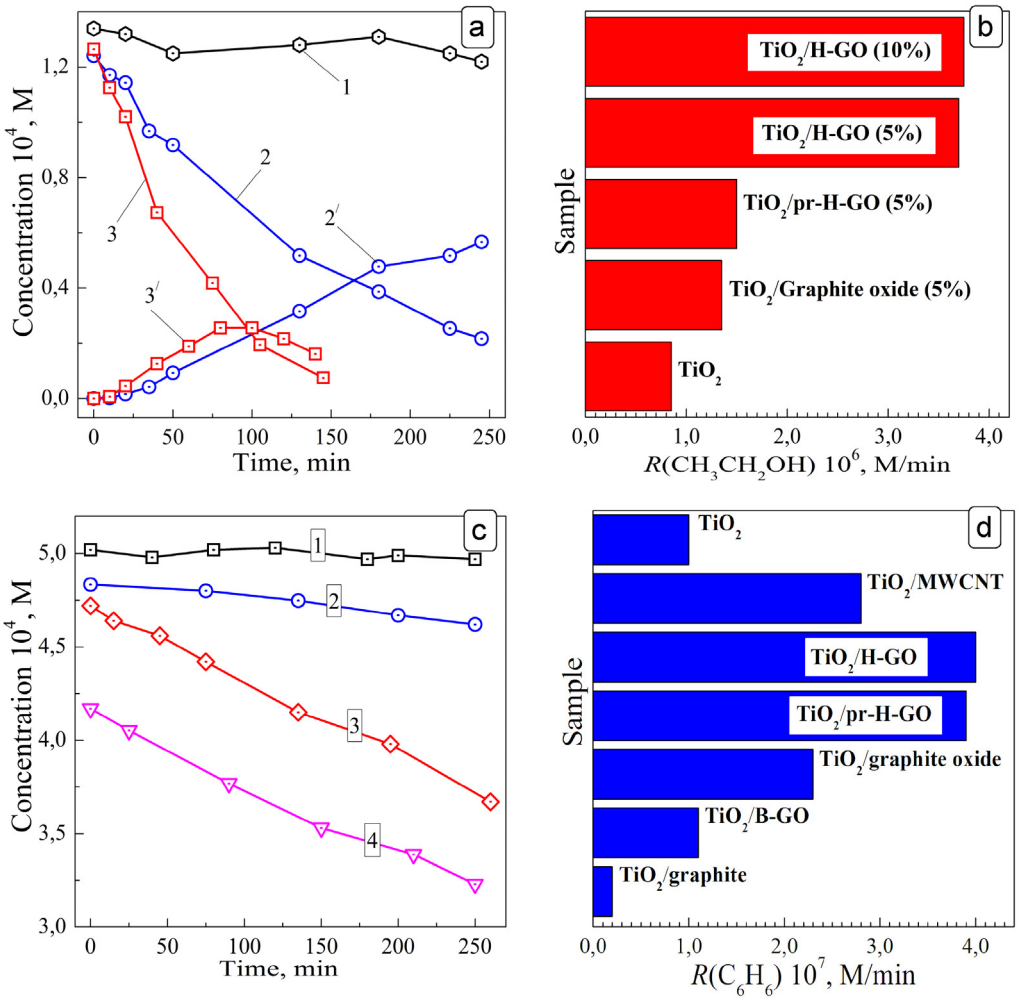

Fig. 2. (a and c) Changes in the concentrations of ethanol (a, curves 1–3), acetaldehyde (a, curves 2′, 3′), and benzene (c) mixed with air under illumination in the absence of photocatalysts (curves 1), in the presence of the P25 titania (curve 2, 2′ in (a); curve 2 in (c)), the TiO_2/H-GO (curves 3, 3′ on (a) and curve 3 on (c)), and TiO_2/pr-H-GO heterostructure (curve 4 on (c)). The H-GO and pr-H-GO content is 5 wt.% (c and d). Rates of photocatalytic oxidation of ethanol $R(CH_3CH_2OH)$ (c) and benzene $R(C_6H_6)$ (d).

indicating a considerably larger amount of the functional groups in the former case, in accordance with the reported data [4,5].

Illumination of the H-GO colloids by UV light induces photoreduction of H-GO sheets, the reduction depth depending on the duration and conditions of the photochemical reaction [30]. Photoreduction results in partial elimination of functional groups and expansion of the aromatic areas of sp^2-hybridized carbon [4,5,30,31,59]. The changes in H-GO structure are evidenced by extinction of the $n\pi$-band, a "red" shift of the characteristic maximum from 230–240 to 260–265 nm and a considerable growth of the visible and near IR absorbance (Fig. 1c, curve 3). The photoreduced H-GO (pr-H-GO) retains monolayer character and stability to aggregation [30].

The nanocrystalline Evonik/Degussa P25 titania is widely used as a *de facto* reference photocatalyst for the benchmarking of photocatalytic properties of various semiconductor nanomaterials and TiO_2-based heterostructures [1,2,63,64]. According to XRD (Fig. 1a, curve 4) the P25 is a mixture of anatase (~80%) and rutile (~20%) with an average coherent scattering domain size of 20–25 nm that reflects the actual size of titania crystallites in the sample. As shown by SEM (Fig. 1d, inset) the P25 consists of loosely aggregated crystals with the size of 20–30 nm, close to that derived from the XRD data. Suspension of the P25 powder in the colloidal GO or pr-GO followed by solvent evaporation does not cause appreciable changes in the sample morphology. After the impregnation, the separate GO (pr-GO) sheets can be observed randomly scattered among the loosely aggregated titania NCs (Fig. 1d).

3.2. Photocatalytic oxidation of ethanol and benzene

Illumination of the nanocrystalline P25 titania by UV light in the presence of ethanol vapors results in a gradual decrease of the alcohol concentration in the gas phase (Fig. 2a, curve 2) and evolution of the two-electron oxidation product – acetaldehyde (Fig. 2a, curve 2′). In a blank experiment (in the absence of photocatalysts) the ethanol concentration remains steady at prolonged illumination (Fig. 2a, curve 1) and no CH_3CHO traces can be detected in the gas phase.

Impregnation of the P25 titania by the colloidal H-GO was found to accelerate the photocatalytic ethanol oxidation considerably (Fig. 2a, curves 3 and 3′). The rate of ethanol photooxidation with participation of the TiO_2/H-GO (5 wt.%) heterostructure is 4 times higher that in the presence of P25 alone. An increase in the H-GO content from 5 to 10 wt.% does not affect appreciably the photoprocess rate (Fig. 2b). Fig. 2b shows that when the non-exfoliated graphite oxide is mixed with P25 titania a much lower photocatalytic reaction rate increment is achieved. A maximum on the curve 3′ (Fig. 2a) indicates that a considerable acceleration of the acetaldehyde formation and oxidation is achieved as well in the presence

Table 1
The rate of photocatalytic benzene oxidation $R(C_6H_6)$.

Sample	Co-catalyst content (wt.%)	$R(C_6H_6) \times 10^7$ ($M \times min^{-1}$)
TiO_2 P25	–	1.0
TiO_2/H-GO	2.5	1.6
TiO_2/H-GO	5.0	4.0
TiO_2/H-GO	7.5	2.1
TiO_2/H-GO	10.0	1.7
TiO_2/pr-H-GO	5.0	3.9
TiO_2/pr-H-GO	10.0	1.0
TiO_2/B-GO	5.0	1.1
TiO_2/graphite oxide	5.0	2.3
TiO_2/graphite	5.0	0.2
TiO_2/MWCNTs	5.0	2.8

of the H-GO sheets. At that, the CH_3CHO consumption competes efficiently with its generation from the photooxidation of ethanol.

At the moment when the adsorption/desorption equilibrium is achieved and illumination is started the ethanol concentration in the gas phase is almost the same for both the P25 titania and the P25/H-GO mixture (curves 2 and 3, Fig. 2a). The fact shows that graphene oxide does not affect appreciably the photocatalyst capability of adsorbing the photoreaction substrate. Besides, the H-GO alone does not manifest photocatalytic properties in the processes under discussion. Therefore, the acceleration of the photocatalytic ethanol and acetaldehyde oxidation by the H-GO originates, most probably, from the active participation of the H-GO sheets in the separation of the charge carriers photogenerated in the TiO_2 NCs. It is reported that the GO sheets, similarly to MWCNTs and fullerenes, can act as electron acceptors [6,7,33] able of capturing the titania conduction band electrons and suppressing the electron-hole recombination. The charge carrier separation is followed, evidently, by the electron transfer from GO to molecular oxygen and generation of the superoxide radicals participating in ethanol and acetaldehyde oxidation [63,64]. Besides, the GO sheets are known to possess inherent catalytic properties toward dehydration and oxidation of various alcohols [65–67].

Preliminary photochemical reduction of the colloidal H-GO results in a considerable decrease of the catalytic activity of H-GO sheets in ethanol and acetaldehyde oxidation. In particular, impregnation of the P25 with the colloidal pr-H-GO gives only a 2-fold increment of the rate of ethanol photooxidation against the 4-fold increase observed in case of the non-reduced H-GO (Fig. 2b). As discussed earlier, the photoreduction of H-GO results in an increase in the GO aromaticity and partial elimination of functional groups. Although the former effect should favor to the capturing and accumulation of the titania conduction band electrons, the latter effect precludes efficient interaction between the pr-H-GO sheets and the surface of TiO_2 NCs and, evidently, dominates in the system under study.

As discussed before, the affinity of a photoreaction substrate to the GO and pr-GO sheets can affect the capability of graphene oxide to accelerate photocatalytic processes. To address this subject we studied the photocatalytic gas-phase oxidation of benzene that, in contrary to ethanol, is potentially capable of selective $\pi\pi$-stacking interactions with the aromatic sections of the GO sheets. It was found that impregnation of the P25 titania with both H-GO and pr-H-GO colloidal solutions results in a considerable, around 4-fold, acceleration of the photocatalytic process as compared with the pure P25 (Fig. 2c, and Table 1), similarly to the above-discussed ethanol photooxidation. No changes in the spectral parameters of absorption spectrum of gaseous reaction mixture were observed during the photocatalytic experiments (Supplementary data (SD), Fig. S1a) indicating that primary products of benzene photooxidation (phenols and any possible ring opening products) are not emitted into the gas phase and are further transformed in the adsorbed state. In the absence of photocatalysts illumination of a mixture of benzene vapors with air does not induce any changes in benzene concentration (Fig. 2c, curve 1; SD, Fig. S1b).

Fig. 2d and Table 1 show that, similarly to ethanol photooxidation, the non-exfoliated multilayer graphite oxide exhibits a much lower catalytic activity in the benzene photooxidation as compared to the activity of monolayer H-GO. The graphite powder, being mixed with the P25 in amount equal to that of H-GO sheets, even inhibits the photocatalytic process. The most probable reason for the inhibition effect is weak interaction between graphite and titania on the background of very good C_6H_6 adsorption on the graphite surface as well as light screening by graphite. Recently we have observed a much more pronounced photochemical activity of GO in acrylamide photopolymerization as compared to both non-exfoliated graphite oxide and pristine graphite [68]. A more pronounced catalytic activity of GO in comparison to graphite as a result of the monolayer character of GO and abundance of functional groups seems to be a general trend supported by DFT calculations [69].

A peak rate of the photocatalytic benzene oxidation is observed at 5 wt.% H-GO sheets in the TiO_2/H-GO composite (Table 1). At a higher H-GO content, 10 wt.%, the photooxidation rate drops more than twice. The same, but much more pronounced effect is observed in case of the pr-H-GO. Here, at an increase in pr-H-GO content from 5 to 10 wt.% the phototransformation rate is reduced by around four times (Table 1).

In the papers reporting the influence of GO and pr-GO on the photocatalytic properties of nanocrystalline semiconductors the importance of comparison of these materials with other carbon nanomaterials able of acting as electron transfer mediators, the MWCNTs in the first place, is stressed upon [12,13,17]. Fig. 2d and Table 1 show that addition of the MWCNTs to the P25 titania actually results in ~3-fold acceleration of the photocatalytic benzene oxidation. The MWCNTs are more active than non-exfoliated graphite oxide but less active than H-GO and pr-H-GO. However, the MWCNTs studied in the present work are agglomerated into tight bundles (SD, Fig. S2) and one may assume that, if properly dispersed, the MWCNTs would exhibit a higher catalytic activity than the colloidal H-GO or pr-H-GO sheets.

A comparison of the curves 1–4 in Fig. 2c in a point corresponding to the adsorption/desorption equilibrium and the beginning of illumination (typically, ~200 min after benzene injection into the reactor) shows that the photoreduced pr-H-GO adsorbs a much higher amount of benzene than the H-GO does. Nevertheless, the photooxidation rate is virtually the same for both TiO_2/H-GO and TiO_2/pr-H-GO composites. The colloidal B-GO, which represents a much deeply oxidized version of graphene oxide as compared to H-GO, was found to have almost no catalytic effect in the system under study. Apparently, the B-GO comprises only a small fraction of aromatic domains of sp^2-hybridized carbon and is not able to accept efficiently the conduction band electrons from the titania NCs.

In both ethanol and benzene oxidation the TiO_2/H-GO heterostructures were found to be a reusable photocatalyst that retains reasonably high activity through several consecutive reaction runs. A loss in photocatalytic activity was found to be around 6–7% in each oxidation cycle. The probable reason for the loss can be partial photoreduction of GO by the conduction band electrons of titania nanocrystals [1,2,33]. As shown above the photoreduction of GO decreases drastically its catalytic activity in ethanol oxidation and can cause an increased light screening effect in the benzene oxidation.

To assess the changes of the GO co-catalyst state during the latter photocatalytic process the TiO_2/H-GO heterostructures were studied by the diffuse reflectance (DRS) and X-ray photoelectron (XPS) spectroscopies. Only very small differences can be observed in the

absorption spectra of TiO_2/H-GO photocatalyst obtained from diffuse reflectance spectra by applying the Kubelka–Munk function before and after the photocatalytic reaction (SD, Fig. S3) indicating that the photoreduction of H-GO, if takes place, is of low efficiency. A survey XPS spectrum (SD, Fig. S4a) shows three groups of signals typical for carbon (C1s), oxygen (O1s) and titanium (Ti2p3/2). The C1s region spectrum (SD, Fig. 4b,c) is characterized by quite a low signal-to-noise ratio, evidently, because of the low H-GO content in the heterostructure studied. Three components can be distinguished in the C1s region of the TiO_2/H-GO sample both before and after the photocatalytic test – the peak of graphitic sp^2-hybridized carbon (~285 eV), carbon bounded to OH group (~286 eV) and a broadened signal centered at 288–289 eV originating from carboxyl groups [70–72]. The intensity ratio of the signals from sp^2-C and C—OH increases slightly, from 0.7 before illumination to 1.1 after the photoprocess completion confirming the above assumption that minor photoreduction of graphene oxide accompanies the main photocatalytic process. The same ratio for pr-H-GO produced by preliminary photoreduction under UV illumination was found to be as high as 6.

In the range of 458–465 eV two peaks were observed at 458.8 eV (Ti2p3/2) and 464.5 eV Ti2p1/2 (SD, Fig. S5a). The peak positions are typical for Ti(IV) in bulk anatase titania [73–75]. The O1p section (SD, Fig S5b) can be deconvoluted into two peaks – at 530 and 532 eV. The first peak can be assigned to OH groups, while the second peak is typical for lattice oxygen in TiO_2 [73–75]. These two section of XPS spectra are absolutely identical for the TiO_2/H-GO sample taken before and after the photocatalytic experiment.

The experimental results on kinetics of the photocatalytic ethanol and benzene oxidation allow to conclude that the activity of the colloidal GO particles as a co-catalyst of the photocatalytic ethanol and benzene oxidation depends on a balance between two factors – (i) aromaticity of the GO sheets and (ii) density of the functional groups decorating the GO sheets. According to the reported data, the deeply oxidized B-GO is characterized by an atomic C:O ratio close to 2:1 and only a residual of the aromatic sp^2-hybridized carbon atoms [4]. By this reason, despite the abundance of the functional groups able of anchoring to the titania NC surface, the B-GO apparently cannot accept efficiently the conduction band electrons from TiO_2 and act as a co-catalyst. In case of the H-GO, synthesized in milder conditions, the C:O ratio is around 3–4:1 and a fraction of sp^2-hybridized carbon atoms varies from 20 to 40% [4]. Evidently, such material can anchor to TiO_2 NCs via hydrogen bonds between the hydroxyl groups on the titania surface and carboxyl/phenol groups of the H-GO sheets and simultaneously has an aromatic system developed enough to accept efficiently the photogenerated conduction band electrons from the TiO_2 NCs. The photoreduction of H-GO results in further expansion of the aromatic areas of the sp^2-hybridized carbon, but at the same time eliminates most of the functional groups [4,30,31]. At that, despite increased electron affinity of the pr-H-GO sheets the interactions between TiO_2 NCs and pr-H-GO become considerably weaker and in general the interfacial electron transfer from TiO_2 NCs to the pr-H-GO sheets becomes less efficient. The extreme case of such tendency is a mixture of TiO_2 with graphite the latter inhibiting photocatalytic activity of the titania NCs.

Obviously, the GO photoreduction results in an increase of its capability of selective adsorption of aromatic substrates, including benzene, which can compensate the losses in the efficiency of the electron transfer. Probably, this compensation effect is responsible for roughly the same catalytic properties of the H-GO and pr-H-GO sheets in benzene photooxidation, while in case of the ethanol oxidation the activity of the two materials is drastically different. A comparatively high catalytic activity of the MWCNTs in the benzene photooxidation speaks in favor to the proposed interpretation. The MWCNT surface is partially covered with the hydroxyl groups as a result of the oxidative post-synthesis etching by nitric acid [56], but at that the MWCNTs retain a partially aromatic character, similarly to H-GO.

The above-discussed interpretation is also indirectly supported by the electrochemical properties of TiO_2/H-GO and TiO_2/pr-H-GO composites. The results of electrochemical measurements are only partially related to the present discussion and therefore are given in Supplementary Data. Analysis of the Mott-Schottky plots obtained for composite film electrodes (SD, Fig. S6a) showed that mixing of the colloidal TiO_2 with the colloidal H-GO (5 w.%) results in a decrease of the titania flat-band potential from −0.9 to −0.5 B (versus Ag/AgCl). At the same time, in the presence of the same amount of photoreduced pr-H-GO the flat-band potential of titania NCs remains almost unchanged. These electrochemical data cannot be unambiguously applied to the P25-based composites discussed in the present work, because the electrochemical experiments were performed on the films produced by mixing the colloidal solutions of TiO_2 and H-GO. The interaction between titania NCs and H-GO sheets in such films is much stronger due to even distribution of non-aggregated TiO_2 NCs over the H-GO sheet surface (SD, Fig. S6b) resulting in a strong influence of graphene oxide on the collective flat-band potential of the whole ensemble of titania NCs. Nevertheless, the electrochemical data strongly suggest that photoinduced elimination of the functional groups from the pr-H-GO sheets results in deterioration of the electron interactions between the pr-H-GO sheets and TiO_2 NCs.

4. Conclusions

Impregnation of the nanocrystalline TiO_2 P25 with the colloidal graphene oxide produced by the Hummers method (H-GO) results in a ~4-fold increase of the rate of photocatalytic gas-phase oxidation of ethanol and benzene by air oxygen. The promoting effect of graphene oxide most probably originates from efficient electron transfer from the photoexcited TiO_2 nanocrystals to H-GO sheets and then – to oxygen molecules. The non-exfoliated multilayer graphite oxide exhibits a much lower activity in the photocatalytic reactions under study.

Preliminary photochemical reduction of colloidal H-GO by UV light results in deterioration of its activity as an ethanol photooxidation co-catalyst but does not affect appreciably the benzene photooxidation rate. At the same time, impregnation of the P25 titania with much deeply oxidized colloidal graphene oxide prepared by the Brodie method (B-GO) gives no acceleration of the photocatalytic oxidation of benzene vapors.

On the basis of the observations it was concluded that the capability of graphene oxide of accelerating the photocatalytic transformations of ethanol and benzene depends on a balance between two factors, in particular, (i) interaction of graphene oxide with the titania nanocrystal surface via anchoring functional groups and (ii) efficiency of accepting of the photogenerated TiO_2 conduction band electrons. The former factor depends on the oxidation state of the graphene oxide sheets and decreases from the most oxidized B-GO to H-GO to the photoreduced H-GO, while the latter factor increases in the same sequence as it depends on the aromaticity of GO sheets.

Acknowledgements

Authors acknowledge financial support of the Research Program of the National Academy of Sciences of Ukraine «Fundamental Problems of Nanostructured Materials, Nanomaterials, and Nanotechnologies» and the Fundamental Research Fund of Ukraine (projects N F41.2/005, F47/20, F53.3/019, F54.3/007). Authors thank Prof. V.L. Karbovskiy and Dr. L.P. Klyuenko (SPM&RS

Center, Kurdyumov Institute of Physics of Metals of Nat. Acad. Sci. of Ukraine) for XPS measurements and Prof. E.A. Streltsov (Belorussian State University, Minsk, Belarus) for electrochemical measurements.

Appendix A. Supplementary data

Supplementary data associated with this article can be found, in the online version, at http://dx.doi.org/10.1016/j.apcatb.2013.11.044.

References

[1] Q. Xiang, J. Yu, M. Jaronec, Chem. Soc. Rev. 41 (2012) 7823–8796.
[2] X. An, J.C. Yu, RSC Adv. 1 (2011) 1426–1434.
[3] N. Zhang, Y. Zhang, Y.-J. Xu, Nanoscale 4 (2012) 5792–5813.
[4] D.R. Dreyer, S. Park, C.W. Bielawski, R.S. Ruoff, Chem. Soc. Rev. 39 (2010) 228–240.
[5] Y. Zhu, S. Murali, W. Cai, X. Li, J.W. Suk, J.R. Potts, R.S. Ruoff, Adv. Mater. 22 (2010) 3906–3924.
[6] G. Eda, M. Chlowalla, Adv. Mater. 22 (2010) 2392–2415.
[7] D.R. Dreyer, R.S. Ruoff, C.W. Bielawski, Angew. Chem. Int. Ed. 49 (2010) 9336–9344.
[8] Q. Xiang, J. Yu, J. Phys. Chem. Lett. 4 (2013) 753–759.
[9] W. Wang, J. Yu, Q. Xiang, B. Cheng, Appl. Catal. B 119–120 (2012) 109–116.
[10] J.S. Lee, K.H. You, C.B. Park, Adv. Mater. 24 (2012) 1084–1088.
[11] L. Ren, X. Qi, Y. Liu, Z. Huang, X. Wei, J. Li, L. Yang, J. Zhong, J. Mater. Chem. 22 (2012) 11765–11771.
[12] H. Zhang, X. Lv, Y. Li, Y. Wang, J. Li, ACS Nano 4 (2010) 380–386.
[13] Y. Zhang, Z.-R. Tang, X. Fu, Y.-J. Xu, ACS Nano 4 (2010) 7303–7314.
[14] C. Chen, W. Cai, M. Long, B. Zhou, Y. Wu, D. Wu, Y. Feng, ACS Nano 4 (2010) 6425–6432.
[15] G. Jiang, Z. Lin, C. Chen, L. Zhu, Q. Chang, N. Wang, W. Wei, H. Tang, Carbon 49 (2011) 2693–2701.
[16] S. Liu, C. Liu, W. Wang, B. Cheng, J. Yu, Nanoscale 4 (2012) 3193–3200.
[17] Y. Zhang, Z.-R. Tang, X. Fu, Y.-J. Xu, ACS Nano 9 (2011) 7426–7435.
[18] M.-Q. Yang, N. Zhang, Y.-J. Xu, ACS Appl. Mater. Interfaces 5 (2013) 1156–1164.
[19] Y.H. Ng, I.V. Lightcap, K. Goodwin, M. Matsumura, P.V. Kamat, J. Phys. Chem. Lett. 1 (2010) 2222–2227.
[20] W. Tu, Y. Zhou, Q. Liu, Z. Tian, J. Gao, X. Chen, H. Zhang, J. Liu, Z. Zou, Adv. Funct. Mater. 22 (2012) 1215–1221.
[21] Y.T. Liang, B.K. Vijayan, K.A. Gray, M.C. Hersam, Nano Lett. 11 (2011) 2865–2870.
[22] W. Fan, Q. Lai, Q. Zhang, Y. Wang, J. Phys. Chem. C 115 (2011) 10694–10701.
[23] H. Kim, G. Moon, D. Monlloe-Satoca, Y. Park, W. Choi, J. Phys. Chem. C 116 (2012) 1535–1543.
[24] Q. Xiang, J. Yu, M. Jaroniec, J. Am. Chem. Soc. 134 (2012) 6575–6578.
[25] Y. Zhang, N. Zhang, Z.-R. Tang, Y.-J. Xu, ACS Nano 6 (2012) 9777–9789.
[26] H. Ma, J. Shen, M. Shi, X. Lu, Z. Li, Y. Long, N. Li, M. Ye, Appl. Catal. B 121–122 (2012) 198–205.
[27] X. An, J.C. Yu, Y. Wang, Y. Hu, X. Yu, G. Zhang, J. Mater. Chem. 22 (2012) 8525–8531.
[28] Q. Li, B. Guo, J. Yu, J. Ran, B. Zhang, H. Yan, J.R. Gong, J. Am. Chem. Soc. 133 (2011) 10878–10884.
[29] O. Akhavan, M. Choobtashani, E. Ghaderi, J. Phys. Chem. C 116 (2012) 9653–9659.
[30] A.L. Stroyuk, N.S. Andryushina, N.D. Shcherban, V.G. Ilyin, V.S. Yefanov, I.B. Yanchuk, S.Ya. Kuchmiy, V.D. Pokhodenko, Theor. Exp. Chem. 48 (2012) 1–11.
[31] Y. Matsumoto, M. Koinuma, S.Y. Kim, Y. Watanabe, T. Taniguchi, K. Hatakeyama, H. Tateishi, S. Ida, ACS Appl. Mater. Interfaces 2 (2010) 3461–3466.
[32] O. Akhavan, ACS Nano 4 (2010) 4174–4180.
[33] G. Williams, B. Seger, P.V. Kamat, ACS Nano 2 (2008) 1487–1491.
[34] Q.-P. Luo, X.-Y. Yu, B.-X. Lei, H.-Y. Chen, D.-B. Kuang, C.-Y. Su, J. Phys. Chem. C 116 (2012) 8111–8117.
[35] Q. Zhang, C. Tian, A. Wu, T. Tan, L. Sun, L. Wang, H. Fu, J. Mater. Chem. 22 (2012) 11778–11784.
[36] S. Liu, Z. Chen, N. Zhang, Z.-R. Tang, Y.-J. Xu, J. Phys. Chem. C 117 (2013) 8251–8261.
[37] Z. Chen, S. Liu, M.-Q. Yang, Y.-J. Xu, ACS Appl. Mater. Interfaces 5 (2013) 4309–4319.
[38] L. Zhang, L. Du, X. Cai, X. Yu, D. Zhang, L. Liang, P. Yang, X. Xing, W. Mai, S. Tan, Y. Gu, J. Song, Physica E 47 (2013) 279–284.
[39] N. Zhang, Y. Zhang, M.-Q. Yang, Z.-R. Tang, Y.-J. Xu, J. Catal. 299 (2013) 210–221.
[40] US Environmental Protection Agency, Masterlist VOCs–Building Assessment Survey and Evaluation. US EPA Washington, DC 20460, 1998 (www.epa.gov).
[41] Occupational Safety and Health Admistration, Limits for Air Contaminants. 1910.1000 Table Z-1, CFR 29. Washington, DC 20210, 1999 (www.osha.gov).
[42] M.R. Nimlos, E.J. Wolfrum, M.L. Brewer, J.A. Fennel, G. Bintner, Environ. Sci. Technol. 30 (1996) 3102–3110.
[43] S. Pilkenton, S.-J. Hwang, D. Raftery, J. Phys. Chem. B 103 (1999) 11152–11160.
[44] C.L. Shao, D.X. Pan, R.X. Zhang, H.Q. Hou, Chem. Papers 61 (2007) 51–54.
[45] B.R. Müller, S. Majoni, D. Meissner, R. Memming, J. Photochem. Photobiol. A 151 (2002) 253–265.
[46] S. Klosek, D. Raftery, J. Phys. Chem. B 105 (2001) 2815–2819.
[47] H. Lu, J. Zhao, L. Li, L. Gong, J. Zheng, L. Zhang, Z. Wang, J. Zhang, Z. Zhu, Energy Environ. Sci. 4 (2011) 3384–3388.
[48] L.-F. Liao, W.-C. Wu, C.-Y. Chen, J.-L. Lin, J. Phys. Chem. B 105 (2001) 7678–7685.
[49] S.-W. Han, J.-H. Lee, J.S. Kim, S.-H. Oh, Y.-K. Park, H. Kim, Environ. Eng. Res. 13 (2008) 14–18.
[50] E. Einaga, S. Futamura, T. Ibusuki, Chem. Lett (2001) 582–583.
[51] Y. Li, N.-H. Lee, D.-S. Hwang, J.S. Song, E.G. Lee, S.-J. Kim, Langmuir 20 (2004) 10838–10844.
[52] H. Huang, X. Ye, H. Huang, P. Hu, L. Zhang, D.Y.C. Leung, Internat. J. Photoenergy (2013), http://dx.doi.org/10.1155/2013/890240 (Article ID 890240).
[53] Y. Ide, N. Nakamura, H. Hattori, R. Ogino, M. Ogawa, M. Sadakane, T. Sano, Chem. Commun. 41 (2011) 11531–11533.
[54] N. Bouazza, M.A. Lillo-Rodenas, A. Linares-Solano, Appl. Catal. B 84 (2008) 691–698.
[55] Y. Ide, M. Matsuoka, M. Ogawa, Chem. Catal. Chem. 4 (2012) 628–630.
[56] N.V. Lemesh, A.I. Tripolskiy, I.E. Kotenko, V.A. Khavrus, P.E. Strizhak, Theor. Exp. Chem. 46 (2010) 288–293.
[57] S. Park, R.S. Ruoff, Nat. Nanotechnol. 4 (2009) 217–224.
[58] C. Botas, P. Alvarez, C. Blanco, R. Santamaria, M. Granda, P. Ares, F. Rodriguez-Reinoso, R. Menendez, Carbon 50 (2012) 275–282.
[59] V.G. Plotnikov, V.A. Smirnov, M.V. Alfimov, YuM. Shulga, High Energy Chem. 45 (2011) 445–449.
[60] D.C. Marcano, D.V. Kosynkin, J.M. Berlin, A. Sinitskii, Z. Sun, A. Slesarev, L.B. Alemany, W. Lu, J.M. Tour, ACS Nano 4 (2010) 4806–4814.
[61] K.A. Mkhoyan, A.W. Contryman, J. Silcox, D.A. Stewart, G. Eda, C. Mattevi, S. Miller, M. Chhowalla, Nano Lett. 9 (2009) 1058–1063.
[62] F. Bonaccorso, Z. Sun, T. Hasan, A.C. Ferrari, Nat. Photon. 4 (2010) 611–622.
[63] K. Nakata, A. Fujishima, J. Photochem. Photobiol. C 13 (2012) 169–189.
[64] W.Y. Teoh, J.A. Scott, R. Amal, J. Phys. Chem. Lett. 3 (2012) 629–639.
[65] D.R. Dreyer, C.W. Bielawski, Chem. Sci. 2 (2011) 1233–1240.
[66] A.D. Todd, C.W. Bielawski, Catal. Sci. Technol. 3 (2013) 135–139.
[67] H.-P. Jia, D.R. Dreyer, C.W. Bielawski, Adv. Synth. Catal. 353 (2011) 528–532.
[68] N.S. Andryushina, O.L. Stroyuk, G.V. Dudarenko, S.Y. Kuchmiy, V.D. Pokhodenko, J. Photochem. Photobiol. A 256 (2013) 1–6.
[69] D.W. Boukhvalov, D.R. Dreyer, C.W. Bielawski, Y.-W. Son, Chem. Catal. Chem. 4 (2012) 1844–1849.
[70] M. Veerapandian, L. Zhang, K. Krishnamoorthy, K. Yun, Nanotechnology 24 (2013) 395706.
[71] A. Hunt, D.A. Dikin, E.Z. Kurmaev, T.D. Boyko, P. Bazylewski, G.S. Chang, A. Moewes, Adv. Funct. Mater. 22 (2012) 3950–3957.
[72] V.H. Pham, H.D. Pham, T.T. Dang, S.H. Hur, E.J. Kim, B.S. Kong, S. Kim, J.S. Chung, J. Mater. Chem. 22 (2012) 10530–10536.
[73] D. Zhang, G. Li, H. Wang, K.M. Chan, J.C. Yu, Cryst. Growth Design 10 (2010) 1130–1137.
[74] D.P. Wang, H.C. Zeng, Chem. Mater. 21 (2009) 4811–4823.
[75] J.K. Zhou, L. Lv, J. Yu, H.L. Li, P.-Z. Guo, H. Sun, X.S. Zhao, J. Phys. Chem. C 112 (2008) 5316–5321.